Comparison of Nanoclay and Carbon Nanofiber Particles on Rheology of Molten Polystyrene Nanocomposites Under Supercritical Carbon Dioxide

Zhihua Guo, Shu-Kai Yeh, Maxwell J. Wingert, Jeffrey L. Ellis, David L. Tomasko, L. James Lee

William G. Lowrie Department of Chemical and Biomolecular Engineering, The Ohio State University, Columbus, Ohio 43210

Received 18 July 2009; accepted 4 October 2009
DOI 10.1002/app.31568
Published online 17 December 2009 in Wiley InterScience (www.interscience.wiley.com).

ABSTRACT: The effects of nanoparticles and high-pressure carbon dioxide (CO_2) on shear viscosity of polystyrene (PS) were studied. Master curves of PS, PS + 5 wt % carbon nanofibers (CNFs), and PS + 5 wt % nanoclay (Southern Clay 20A) without CO_2 were created based on parallel-plate measurements. The results showed that addition of nanoparticles increased the viscosity of the neat polymer. Steady-state shear viscosity of PS in the presence of CO_2 and nanoparticles was measured by a modified Couette rheometer. The effect of supercritical CO_2 on these systems was characterized by shift factors. It was found that under the same temperature and CO_2 pressure, CO_2 reduced the viscosity less for both PS-20A and PS-CNFs than neat PS. Between the two types of nanoparticles, CNFs showed a larger viscosity reduction than 20A, indicating a higher CO_2 affinity for CNFs than 20A. However, the advantage of CNFs over 20A for larger viscosity reduction decreased with higher temperature. A gravimetric method (magnetic suspension balance) was used to measure the excess adsorption of CO_2 onto CNFs and nanoclay, thus, CO_2 showed a higher affinity for CNFs. © 2009 Wiley Periodicals, Inc. J Appl Polym Sci 116: 1068–1076, 2010

Key words: rheology; nanoparticles; nanoclay; carbon nanofibers (CNFs); carbon dioxide; polystyrene; Couette rheometry; shear viscosity; shift factor

INTRODUCTION

Application of supercritical carbon dioxide in PS nanocomposite foaming

A wide variety of polymers are used for foaming applications, such as polyurethane (PU), polyisocyanurate (PIR), polystyrene (PS), polyolefin, poly(vinyl chloride) (PVC), and epoxy. According to the 2001 U.S. polymer foam market report, PS foam possessed about 26% of the market, second only to PU (53%).[1] PS foams are used in a variety of applications, such as cushioning, thermal insulation, packaging, structural components, and marine applications.[2] As one of the most versatile thermoplastic resins available for the production of low-cost plastic foams, there is strong interest in its development.

With the ban on chlorofluorocarbons (CFCs) and the impending phase-out of hydrochlorofluorocarbons in 2010,[3] there has been significant investment in alternative physical blowing agents. Nitrogen is an attractive alternative, because it is inexpensive and inert but its low solubility necessitates very high-pressure operation. Water is also attractive for the same reasons but its low volatility presents engineering challenges and it is corrosive at extrusion temperatures. Carbon dioxide (CO_2), hydrofluorocarbons, and hydrocarbons come the closest to provide the characteristics required by current processes and are in current development as replacement blowing agents. Our work has focused on the use of CO_2 in foam applications to fully exploit its safety and cost advantages over flammable materials and its cost and environmental benefits over hydrofluorocarbons.

Many different types of polymers have proven amenable to foam with CO_2 and for some applications, such as structural foam insulation, the challenges that persist include dimensional instability during the foam-shaping process and poor control of cell size and density. These partially result from the relatively high diffusivity of CO_2 out of the polymer during foaming.

Polymer nanocomposites have been proposed to overcome some of these drawbacks. Polymer nanocomposites refer to a class of reinforced polymer with a low percentage of well-dispersed particles

Correspondence to: D. L. Tomasko (tomasko@chbmeng.ohio-state.edu).

Contract grant sponsor: National Science Foundation (Center for Advanced Polymer and Composite Engineering (CAPCE) at The Ohio State University); contract grant number: DMI-0602911.
Contract grant sponsor: Owens Corning.

with at least 1 nm-sized dimension. A small amount of well-dispersed nanoparticles in the polymer may serve as nucleation sites to facilitate the cell nucleation process. The presence of nanoparticles may enhance mechanical and physical properties, heat distortion temperature, and fire resistance of polymer foams.[4] In addition, plate-like nanoparticles may reduce gas diffusivity in the polymer matrix.[5]

There are three different types of nanoparticles[4] used for fabrication of nanocomposites. The first type is plate-like with a thickness in the nanometer range and lateral dimensions in the range from several hundred nanometers to a few micrometers. Clays are a good example. An organically modified nanoclay, Cloisite 20A (20A for short), was used to fabricate nanocomposites in this work. The second type has an elongated structure (fiber or tube shaped) with two dimensions at the nanometer scale, such as carbon nanofibers (CNFs) and carbon nanotubes (CNTs). The third type has all three dimensions in the range of nanometer, such as spherical silica particles.

In general, the foaming process comprises three fundamental steps: cell nucleation, cell growth, and cell stabilization. The rheological behavior of polymers in the presence of a blowing agent directly affects the cell growth rate and cell stabilization, both of which have a strong impact on the final cell morphology. In particular, the extrusion foaming process is largely controlled by the complex rheological behavior of the polymer-blowing agent mixture.

Viscosity reduction of polymer nanocomposites by CO_2

Time–temperature superposition is commonly used in polymer rheology to generate master curves. Similarly, this concept has been extended to generate a master curve using pressure and CO_2 concentration. Various research groups[6–15] have shown that the viscosity reduction of polymer melts in the presence of dissolved CO_2 could be described in terms of viscosity scaling theory. Gerhardt et al.[7] have shown that classical viscoelastic scaling factors can be used to superpose the viscosity curves for CO_2-swollen melts onto the viscosity curve for pure polydimethylsiloxane (PDMS) at the same temperature and pressure. They combined a free volume expression for the viscosity of a diluted polymer melt with equation-of-state theories for the volumetric properties of PDMS-CO_2 mixtures to develop models for the CO_2 concentration-dependent viscoelastic scaling factors. The free volume theory of Gerhardt et al.[7] was used by Kwag et al.[8] to predict viscoelastic scaling factors describing the effect of CO_2 concentration on the viscosity curves of PS melts. Lee et al.[9] proposed a model using the generalized Cross-Carreau equation and Doolittle's free volume theory to describe the viscosity of PS-CO_2. Recently, Royer et al.[13] developed a free volume model (WLF-Chow equation) based on the Williams–Landel–Ferry (WLF)[16] equation. The WLF-Chow equation is widely used to calculate the pressure shift factor a_P, concentration shift factor a_v, and their combination $a_P \cdot a_v$. The equations are as follows:

$$\log(a_P) = \log\left(\frac{\eta(T,P,c)}{\eta(T,P_0,c)}\right) = \frac{c_1(T - T_{g,\mathrm{mix},P_0})}{c_2 + T - T_{g,\mathrm{mix},P_0}} - \frac{c_1(T - T_{g,\mathrm{mix},P})}{c_2 + T - T_{g,\mathrm{mix},P}} \quad (1)$$

$$\log(a_c) = \log\left(\frac{\eta(T,P_0,c_0)}{\eta(T,P_0,c)}\right) = \frac{c_1(T - T_{g,P_0})}{c_2 + T - T_{g,P_0}} - \frac{c_1(T - T_{g,\mathrm{mix},P_0})}{c_2 + T - T_{g,\mathrm{mix},P_0}}, \quad (2)$$

where η is shear viscosity, T is temperature, P and P_0 are pressure and reference pressure, respectively, c_1 and c_2 are constants in WLF equation, c and c_0 are concentration of the diluent in the polymer matrix and reference concentration, respectively, and $T_{g,\mathrm{mix}}$ is the glass transition temperature of the mixture. The first shift factor accounts for hydrostatic pressure with a known concentration of diluent, whereas the second equation removes the concentration to allow direct comparison with diluent-free atmospheric-pressure viscosity. The structure of the equations is similar to those given by Penwell and Porter.[17] It does not rely upon any *P-V-T* data other than specifying the T_g change with pressure and concentration. The latter is governed by the Chow model.[18]

Most experimental studies in the literature used slit and capillary dies, which provide data at high shear rates. However, their limitation is that the large pressure drop across a capillary or slit die limits the concentration of diluent that can be dissolved in the polymer melt, as to ensure no phase separation occurs. A backpressure regulator or nozzle can be used to keep the diluent in the solution and to control the die flow resistance. The meaning of individual viscosity measurements from these methods is complicated by the fact that they correspond to a range of pressures rather than representing viscosity at a particular pressure. Several studies[10–14] have investigated the viscosity of PS/CO_2.

Rotational rheometers overcome the problem of average pressures by allowing the polymer to come to equilibrium with the diluent. Furthermore, they have the ability to measure low shear rates that often approach the Newtonian regime (zero-shear viscosity). Flichy et al.[19] measured the viscosities of polymer-inorganic suspensions under CO_2, but they

were forced to approximate the average shear rate, because they used vanes to generate shear. Oh et al.[20,21] constructed a high-pressure Couette rheometer and measured Newtonian viscosities of PS-CO_2. The shear viscosities of PS-CO_2 at 130–200°C and 10–20 MPa were measured. Viscosity curves under different temperatures and pressures fall on a master curve and demonstrate the advantages of Couette measurements for polymer-supercritical fluid systems. Wingert et al.[15] systematically studied the shear viscosity of PS-CO_2 by a modified Couette rheometer. Shear viscosity of PS-CO_2 was measured from 140 to 180°C and from 0 to 6 wt % CO_2. The pressure effect was studied by measuring the shear viscosity of PS under an insoluble gas (Helium). Several shift factors, $a_P \cdot a_c$, a_P, and a_c, were compared with the prediction by WLF-Chow model. Qualitative agreement was achieved.

In previous studies by our group, 20A[22,23] and CNFs[24–26] were used as additives/nucleation agents in PS foaming. In the complex nanocomposite foaming process, several operating variables (e.g., temperature, pressure, and pressure drop rate) and material-related properties (e.g., solubility, diffusivity, and viscosity) are interrelated. In this study, we are interested in how the viscosity of polymer nanocomposites based on plate-like particles (20A) and fiber-like particles (CNF) compare under high-pressure CO_2. This may explain observed differences in cell growth rate and foam morphology.

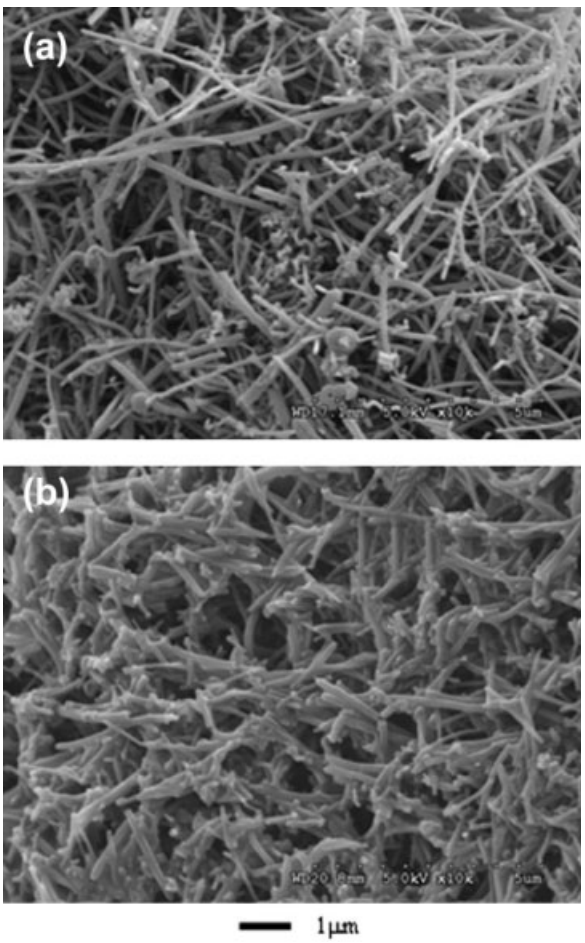

Figure 1 Representative SEM images for CNFs: (a) raw and (b) by microcompounding (the PS + 5% CNFs sample was dissolved by THF to remove PS and then centrifugated).

EXPERIMENTAL

Materials

PS (CX5197) was obtained from Total Petrochemicals and used as received without further purification. Zinc stearate, a common lubricant/plasticizer found in many commercial PS grades, was not present in CX-5197. CO_2 (>99.9%) was supplied by Praxair.

Vapor grown CNFs (PR-24-PS, supplied by Applied Science) were pyrolytically stripped to remove the surface organic contamination. The average diameter of these CNFs was 100 nm and the original length ranged from 30 to 100 μm. For melt blending, PS + 5 wt % CNFs (volume fraction: 2.7%) nanocomposite, CNF powder, and PS pellets were fed into a DACA microcompounder, a small twin-screw extruder in which the compounding time, temperature, and screw speed can be controlled. Samples were compounded for 3 min at 180°C and 150 rpm. We refer to this material as "microcompounded PS + 5% CNFs." To check the length of CNFs after compounding, the sample was dissolved in THF (tetrahydrofuran), centrifuged, and placed on stubs for SEM analysis (HITACHI S-4300). As shown in Figure 1, CNFs were severely shortened by the shearing of the microcompounder, with an average length of only 2.6 μm by analyzing SEM images. Pure PS was also processed through the microcompounder at the exact same condition for comparison with PS + 5 wt % CNFs and is referred to as "microcompounded PS."

The PS + 5 wt % 20A (volume fraction: 2.0%) nanocomposite was mechanically blended at 200°C using a twin-screw extruder (Leistritz ZSE-27; $L/D = 40$; $D = 27$ mm; screw speed 300 rpm) and pelletized. This will be referred to as "extruded PS + 5% 20A." Pure PS was also processed through the extruder with the exact same condition for comparison with PS + 5 wt % 20A. This will be referred to as "extruded PS."

To compare the rheological behavior between PS, PS + 5% CNFs, and PS + 5% 20A, it is ideal to use the exact same processes and conditions for all three systems. However, the extruder was not used to fabricate PS + CNFs composite because of the large amount of CNFs required (due to high price of CNFs) and the severe shortening of CNFs length by

higher shear rate in the extruder. Moreover, we have a good knowledge of the rheological properties of the PS + CNFs made by the same procedure (microcompounding).[27] It should still be appropriate to compare the effects of 20A and CNFs even though we used different processes if we compare the PS composites to the corresponding PS with the same processing history.

CO_2 adsorption was measured on CNFs and also on nanoclay (montmorillonite (MMT) Na^+ untreated) supplied by Southern Clay. Both were used as received. CO_2 (>99.99%) and helium (>99.999%) were supplied by Praxair.

Apparatus

The rheometer (model: MCR 500) is manufactured by Anton Paar. This controlled-stress rheometer measured steady shear viscosities and shear rates by setting a constant torque and measuring angular motion. The manufacturer's software was used to calculate shear stress and shear rate. Its frequency range is from 0.0001 to 100 Hz, according to the manufacturer, and relies upon an air bearing for its precision. This study used parallel plates operated in oscillatory mode and a modified Couette high-pressure cell operated in constant stress mode.

High-pressure measurements used a Couette geometry that houses an inset cup and bob inside a high-pressure cell. Some changes were made to the high-pressure cell to raise pressure and to improve thermal uniformity. These specifics are available in a previous study.[15] The cell holds pressures up to 20 MPa and a burst disc is used for safety. High-pressure CO_2 was delivered to the high-pressure vessel via an ISCO 500D syringe pump. The pressure was detected by a Honeywell Sensotec AG400.

A magnetic suspension balance (MSB) manufactured by Rubotherm was used to measure sorption of CO_2 on nanoparticles. The MSB was equipped with a high-pressure/temperature view cell. The cell can be operated at pressures up to 15 MPa and temperatures up to 150°C and has a mass resolution of 10 μg. The pressure was controlled by an ISCO Syringe Pump (500D) to ±0.001 MPa, and a vacuum pump (The Welch Scientific Company 1400) was used for pressures below ambient. The temperature was controlled by a Julabo Circulator (F25-ME) that pumped heating fluid through a thermal jacket, which surrounded the high-pressure cell, to ±0.01°C. The pressure and mass data were logged on the computer using the MessPro software from Rubotherm, and the temperature data were logged using the Julabo Easy Temp software. More details on the internal workings of the MSB can be found in the literature.[28]

Experimental procedure

To generate an ambient pressure viscosity master curve, the parallel-plate geometry was used. Thin (about 1 mm) circular discs of polymer or polymer nanocomposites were made by compression molding (180°C) under the protection of nitrogen. For measurement, the rheometer was operated in oscillatory mode also under protection of nitrogen to minimize degradation.

For the high-pressure measurement, the Couette geometry was used. Detailed operating procedures are mentioned elsewhere.[15] Only a brief description is given here. An extremely long diffusion and equilibrium time (several months) was significantly shortened by introducing a porous cup made of sintered 316 stainless steel. The porous cup allowed CO_2 to quickly distribute to all the sides and even the bottom of the polymer melt. The fact that the porous cup produced statistically equivalent data with the solid cup at ambient pressure proved that the porous cup did not affect the measurement. A minimum of 50-h equilibration time was used at each combination of temperature and CO_2 pressure to ensure equal distribution of CO_2 in the polymer. During the equilibration time, the temperature was maintained at 150°C to suppress degradation. Then, the temperature was raised to the desired level, and pressure was adjusted simultaneously to maintain the CO_2 concentration. In the whole measurement, PS was either protected by nitrogen or in high-pressure CO_2 to minimize oxygen-induced degradation. In addition, minimizing exposure to high temperature during the 50-h equilibration time helped to minimize degradation.

For PS and PS nanocomposites, each sample was tested at three temperatures (180, 190, and 200°C) and four concentrations (0, 3, 4, and 5 wt % CO_2). The appropriate pressure to achieve the desired CO_2 concentration at a particular temperature was determined by the Sanchez-Lacombe equation-of-state.[29] It was correlated to an experimental PS sorption study by Sato et al.[30] The same pressure was used for PS and PS nanocomposites to achieve the same CO_2 concentration in PS or PS matrix in the two nanocomposites.

The MSB was used to measure the excess adsorption of CO_2 on both CNF and nanoclay (untreated) at 35°C. The CO_2 was allowed to reach adsorption equilibrium (>12 h) with the nanoparticles for every 1 MPa up to 7 MPa. A buoyancy force correction was made at each point based on the fluid density and the volume of the sample. The fluid density was measured *in situ*,[28] and the volume of the sample was measured using a high-pressure helium technique.[31] The sample was contained in a sintered 316 stainless steel container during the measurement so

that CO_2 could diffuse through it, but nanoparticles could not escape.

The physisorption of nitrogen using an ASAP 2010 (Micromeritics) was analyzed using the Brunauer-Emmett-Teller method to establish the surface area of the materials studied.

RESULTS AND DISCUSSION

Figure 2 shows master curves for extruded PS + 5% 20A, as-received PS, extruded PS, microcompounded PS + 5% CNFs, and microcompounded PS (from top to bottom) with a reference temperature of 200°C in the absence of any CO_2. Comparing the master curves of extruded PS and extruded PS + 5% 20A, the addition of nanoclay causes a significant viscosity increase. Similarly, addition of CNFs increases viscosity when comparing the curves of microcompounded PS and PS + 5% CNFs. Furthermore, when comparing as-received PS with either extruded or microcompounded PS, significant degradation occurs in the latter two. Surprisingly, microcompounding results in even more severe degradation than extrusion in this case. In the extrusion process, 200°C and 300 rpm were used; in the microcompounding, 180°C and 150 rpm were used. Because of higher temperature and higher rpm, more degradation was expected in the extrusion process. The possible reason that microcompounding leads to more degradation than extrusion is the residence time in the process. In the microcompounding, after 3 min of mixing, the motor was stopped and then the sample (3 g each batch) was extruded out. For extrusion, the residence time was less than 3 min due to the high rpm used. In other words, longer residence time in the microcompounder could lead to more severe degradation. This demonstrates the importance of processing history (e.g., heat, shear) for viscosity studies. In addition, different processes lead to various fiber orientation, therefore, rheological and other properties.[32]

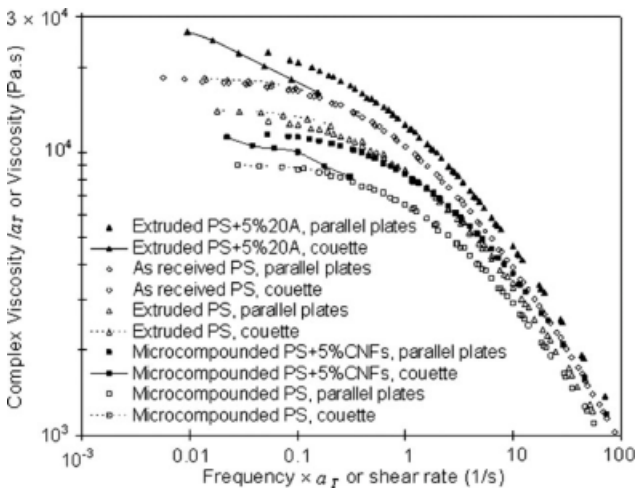

Figure 2 Master curves of shifted complex viscosity versus frequency at reference temperature 200°C for microcompounded PS, microcompounded PS + 5% CNFs, extruded PS, as-received PS results taken from the literature,[15] and extruded PS + 5% 20A along with corresponding steady shear viscosity measurements from the Couette rheometer.

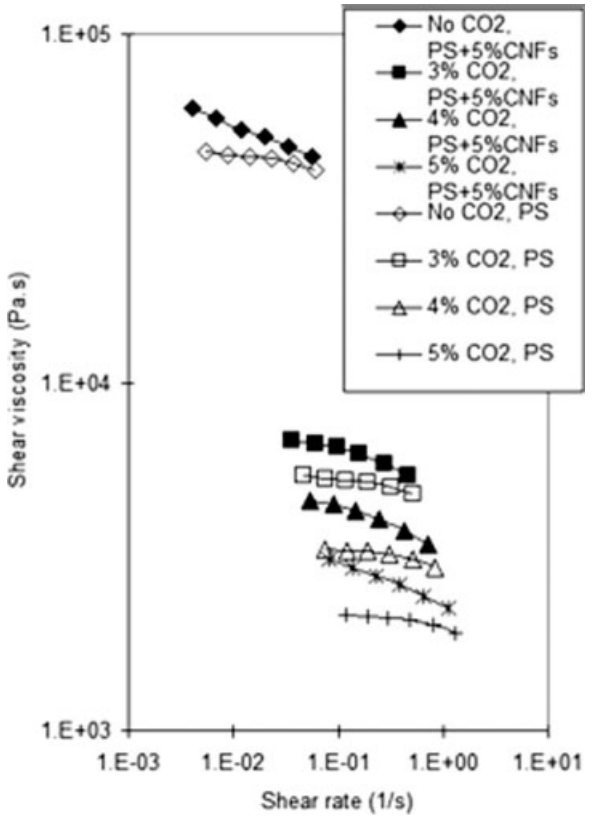

Figure 3 Shear viscosity of microcompounded PS + 5% CNFs and microcompounded PS at 180°C under different CO_2 concentration (0, 3, 4, and 5 wt %).

Figure 2 also shows the steady shear viscosities from the Couette rheometer. The Cox–Merz relationship[33] is invoked to compare the parallel-plates master curves and Couette viscosities. For the three pure PS results, reasonable agreement between the two techniques is observed. For the two nanocomposites, the Couette viscosities show more shear thinning at the shear rates investigated (order of 0.1 s^{-1}) than do the master curves. This suggests that the Cox–Merz relationship does not apply for these two melt-blended 95% PS and 5% nanoparticle composites. One possibility is that the presence of a yield stress in the nanocomposites prohibits the use of the Cox–Merz relationship.[34,35]

Figures 3 and 4 show the shear viscosity of PS + 5% CNFs and PS + 5% 20A, respectively, at 180°C

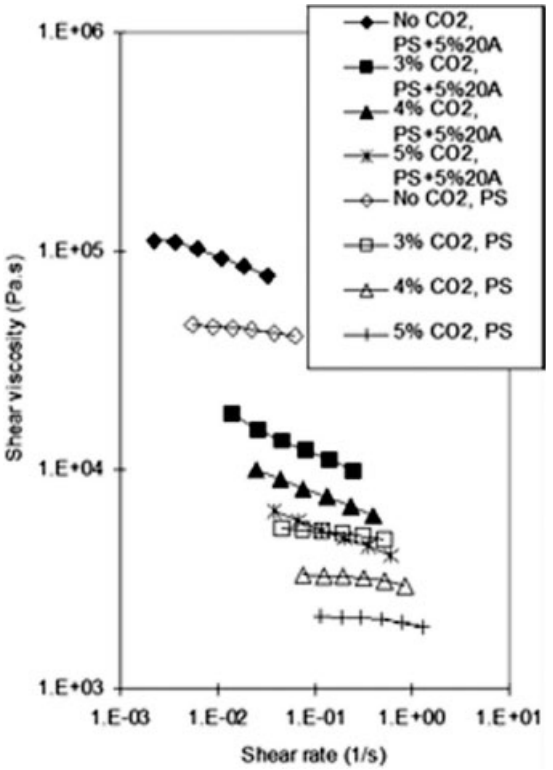

Figure 4 Shear viscosity of extruded PS + 5% 20A and extruded PS at 180°C under different CO_2 concentration (0, 3, 4, and 5 wt %).

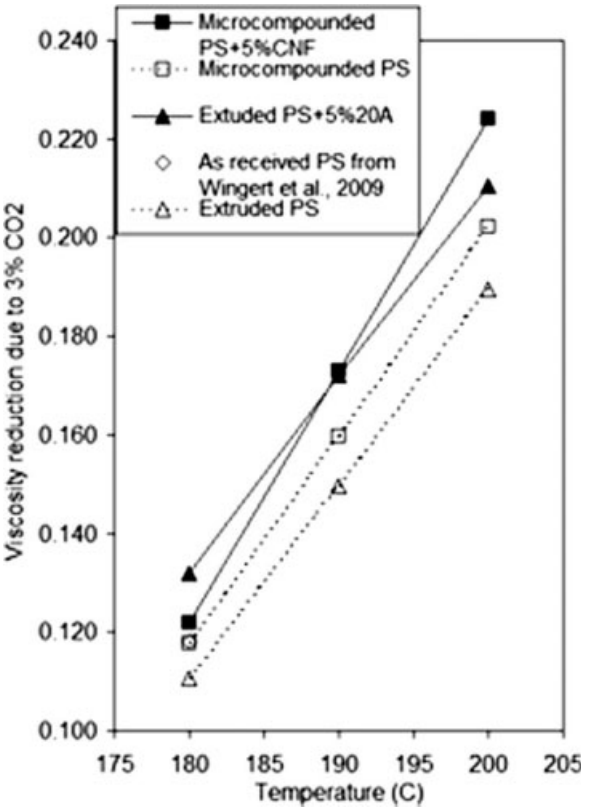

Figure 5 Shift factor $a_P \cdot a_c$ of extruded PS, extruded PS + 5% 20A, microcompounded PS, and microcompounded PS + 5% CNFs at 3% CO_2.

under different CO_2 concentration (0, 3, 4, and 5 wt %). In general, with the addition of either CNFs or 20A, the viscosity of the PS is higher than the neat PS with or without CO_2. The same trend is shown for data at 190 and 200°C. To compare the effect of CO_2 on these systems, we calculated the values of $a_P \cdot a_c$. The $a_P \cdot a_c$ shift factor can be obtained by forming a master curve of viscosity-shear rate data with and without high-pressure CO_2. Viscosity was shifted to an equal amount on both axes to produce a plot of $\eta/a_P \cdot a_c$ versus $\dot{\gamma} \cdot a_P \cdot a_c$ at a given temperature.

The viscosity reduction due to CO_2, $a_P \cdot a_c$, is shown in Table I at 180°C for the three PS materials. In our previous study,[15] this high-pressure, high-temperature PS rheology method demonstrated insignificant degradation when using a careful heating strategy as long as 10 days. In this study, the same procedure was used, but the viscosity was measured at temperatures up to 200°C. It appears that the higher temperatures used in this study lead to somewhat more degradation than in the previous study, because the 4 and 5% concentration results that represent the longest durations under high temperature (the three concentrations from this study were measured in ascending order) show lower values of $a_P \cdot a_c$ than our previous study. At most, for 5% CO_2, the extruded PS sample results in a 23% lower viscosity shift factor than our previous study. It is

TABLE I
Comparion of Viscosity Reduction Due to Carbon Dioxide at 180°C for Three Polystyrene Materials

CO_2 content (wt %)	$a_P a_c$ of as-received PS[a]	$a_P a_c$ of extruded PS	$a_P a_c$ of microcompounded PS
3	0.118	0.111	0.118
4	0.0737	0.0661	0.0727
5	0.0530	0.0402	0.0472

[a] Taken from Ref. 15.

TABLE II
Molecular Weight Distribution by Size Exclusion Chromatography for PS (As-Received), PS in Compounded PS + 5% CNFs Before and After Rheology Test

Sample	M_w	M_n	M_z	D
PS as-received	162,900	66,830	395,200	2.44
PS in nanocomposite before Couette test	135,800	62,820	294,600	2.16
PS in nanocomposite after Couette test	130,700	60,140	307,200	2.18

Conditions: columns: TSK 1000, 3000, and 6000 HXL 30CM; solvent: tetrahydrofuran; rate: 1.0 mL/min; injection volume: 50 μL; detectors: RI at 254 nm; concentration: 1.0%; calibration: based on PS standards; precision: ±10–15% relative.

plausible that degradation is the cause for these results because degradation directly affects the calculation of the shift factors. Thus, Figure 5 shows $a_P \cdot a_c$ for 3% CO_2, where the degradation has the smallest impact on the data. Reasonable agreement exists between the three PS samples.

The CNF nanocomposite, the as-received PS, PS separated from the compounded PS + 5% CNFs sample, and the same sample after the multiday measurement were analyzed by size exclusion chromatography for molecular weight distribution. The PS was separated from the nanocomposite using dissolution in THF and centrifugation. Table II shows that there is some decrease in molecular weight due to the long measurement, but it is relatively insignificant. The molecular weight change due to the compounding process was much more significant. Thus, we can expect the viscosity impact of degradation due to the multiday CO_2 experiment to be much smaller than the viscosity difference between the as-received and microcompounded viscosities shown in Figure 2.

Figure 5 compares the viscosity reduction due to 3 wt % CO_2 of the two nanocomposites to that of PS. The addition of both fillers increases the shift factor, meaning the viscosity is reduced less under high-pressure CO_2. This also means that the effectiveness of high-pressure CO_2 on reducing viscosity is slightly diminished for these materials. To compare the viscosity reduction between two types of nanoparticles 20A and CNFs, we should not compare $a_P \cdot a_c$ directly due to the difference of fabrication of these two composites. The appropriate way is to compare PS composites with corresponding PS. From Figure 5, we can conclude: at 180°C, addition of CNFs shows larger viscosity reduction than 20A, whereas at 200°C the 20A nanocomposite shows similar viscosity reduction. Figure 6 shows the viscosity reduction at 180, 190, and 200°C with three different CO_2 weight fractions. We can draw the following two conclusions. First, for all temperatures, addition of CNFs shows larger viscosity reduction than 20A (or at least similar in one case). Second, for each CO_2 weight fraction, the advantage of CNFs over 20A for larger viscosity reduction decreases with higher temperature. In addition, the impact of nanocomposites on the high-pressure CO_2 shift factor is relatively small, but it is statistically

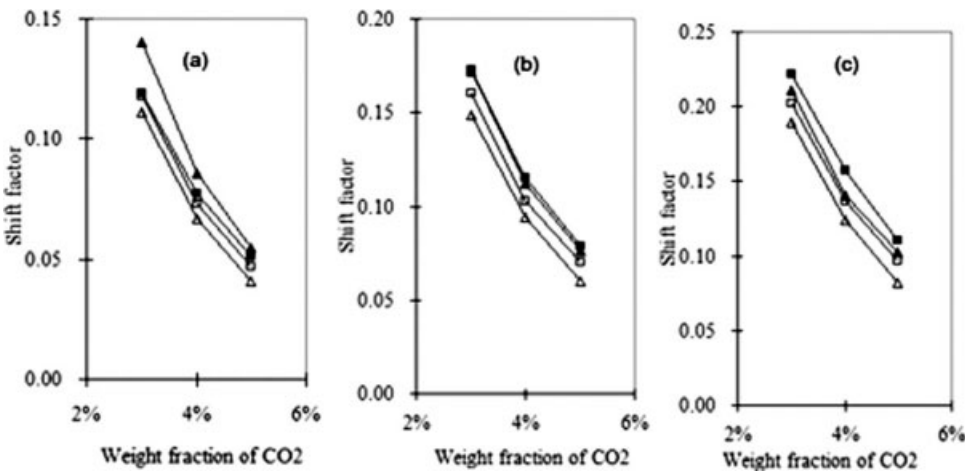

Figure 6 Shift factor $a_P \cdot a_c$ of extruded PS (empty triangles), extruded PS + 5% 20A (filled triangles), microcompounded PS (empty squares), and microcompounded PS + 5% CNFs (filled squares) at 180°C (a), 190°C (b), and 200°C (c).

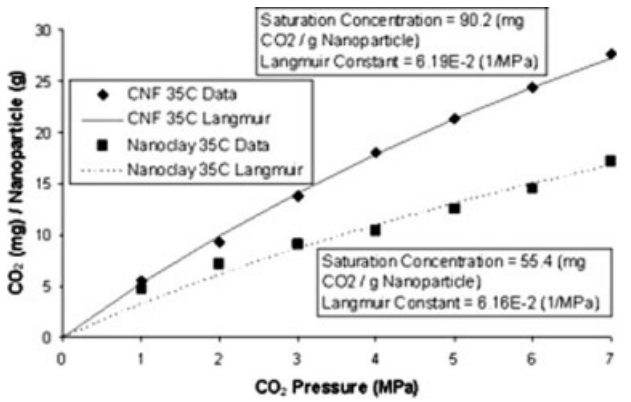

Figure 7 CO_2 excess adsorption on nanoclay (untreated) and CNF at 35°C with Langmuir isotherm fitting parameters shown.

significant. Because the same equilibration pressure was used for PS and each of the nanocomposites, the actual amount of CO_2 in the nanocomposites might be slightly higher because the affinity of the nanoparticles for CO_2 will attract CO_2 molecules to the polymer-particle interface, whereas the CO_2 content in the bulk polymer is unaffected by the presence of nanoparticles. However, other measurements of CO_2 solubility in nanocomposites have shown no significant increase over pure polymer. Nonetheless, if CO_2 partitions to the interface, it could certainly impact the viscosity results.

It is helpful to know which of the two nanoparticles has a higher CO_2 affinity. Thus, adsorption data for CO_2 on CNFs and montmorillonite nanoclay under high pressure were obtained at 35°C (the lower temperature was due to equipment limitations). The only difference between montmorillonite nanoclay and 20A is the surface treatment. The surface chemistry for montmorillonite is simply Na^+, and for 20A it is an alkyl-chain quaternary ammonium salt. Although the excess adsorption data would be expected to differ between Na^+ and 20A, we expect the comparison between CNFs and Na^+ to adequately represent the difference in CO_2 affinity between CNFs and 20A. The results are shown in Figure 7. Each set of data was fit to a Langmuir isotherm, where the saturation concentration and Langmuir constant were quantified. It is clear that CO_2 has a greater affinity for the CNFs over the nanoclay (untreated) by both the qualitative shape of the excess adsorption isotherm and the quantitative values of the Langmuir constants. The greater affinity for the CNFs over the nanoclay is partially due to the fact that the former has much higher surface area per mass. As shown in Table III, CNFs have more surface area than either of the nanoclay samples. The larger surface area available on the CNFs may be the reason that they are able to adsorb more CO_2.

Our rheology data might be explained by a higher CO_2 content at the interface of PS/CNFs than for PS/20A. A higher CO_2 content at the particle/polymer interface might lubricate the flow similar to the interfacial slip observed in liquid crystalline polymers[36–38] and immiscible polymers.[39]

CONCLUSIONS

The extrusion foaming process, as well as the final foam structure, is largely controlled by the complex rheological behavior of PS-CO_2-nanoparticle mixtures. In this study, master curves of PS, PS + 5 wt % CNFs, and PS + 5 wt % 20A without CO_2 were formed based on parallel-plate measurements. The results showed that addition of nanoparticles increased the viscosity of the neat polymer. The results also showed that Cox–Merz relationship does not apply for the two melt-blended 95% PS and 5% nanoparticle composites. In addition, to have a better understanding of the foaming process, steady-state shear viscosity of PS in the presence of the blowing agent CO_2 and nanoparticles was measured by a modified Couette rheometer. The effect of high-pressure CO_2 on these systems was characterized by shift factors. Under the same temperature and CO_2 pressure, CO_2 reduced the viscosity less for both PS-nanoclay and PS-CNFs than neat PS. Between the two types of nanoparticles, addition of CNFs showed larger viscosity reduction than 20A, indicating a higher CO_2 affinity for CNFs than 20A. However, the advantage of CNFs over 20A for larger viscosity reduction decreased with higher temperature. The higher CO_2 affinity toward CNFs was also confirmed using adsorption data.

TABLE III
Surface Areas for CNFs, Untreated Nanoclay, and Treated Nanoclay (20A)

Nanoparticle	BET surface area (m^2/g)	Langmuir surface area (m^2/g)	Density (g/cm^3)
Nanoclay (untreated)	12.5	14.5	2.65
Carbon nanofiber	58.5	86.5	1.97
Nanoclay (Cloisite 20A)	12.6	19.5	No data

The authors thank Owens Corning for material donation and molecular weight distribution measurement.

References

1. Forman, C. RP-120X Polymeric Foams—Updated Edition; Business Communications Company, Inc.: Norwalk, CT, 2001.
2. Klempner, D.; Frisch, K. C., Eds. Handbook of Polymeric Foams and Foam Technology; Oxford University Press: Munich, 1991.
3. UNEP. The Montreal Protocol on Substances that Deplete the Ozone Layer; UNEP: Nairobi, Kenya, 2000.
4. Lee, L. J.; Zeng, C.; Cao, X.; Han, X.; Shen, J.; Xu, G. Compos Sci Technol 2005, 65, 2344.
5. Guo, Z.; Lee, L. J.; Tomasko, D. L. Ind Eng Chem Res 2008, 47, 9636.
6. Nalawade, S. P.; Nieborg, V. H. J.; Picchioni, F.; Janssen, L. P. B. M. Powder Technol 2006, 170, 143.
7. Gerhardt, L. J.; Garg, A.; Manke, C. W.; Gulari, E. J Polym Sci Part B: Polym Phys 1998, 36, 1911.
8. Kwag, C.; Manke, C. W.; Gulari, E. Ind Eng Chem Res 2001, 40, 3048.
9. Lee, M.; Park, C. B.; Tzoganakis, C. Polym Eng Sci 1998, 38, 1112.
10. Areerat, S.; Nagata, T.; Ohshima, M. Polym Eng Sci 2002, 42, 2234.
11. Kwag, C.; Manke, C. W.; Gulari, E. J Polym Sci Part B: Polym Phys 1999, 37, 2771.
12. Lee, M.; Park, C. B.; Tzoganakis, C. Polym Eng Sci 1999, 39, 99.
13. Royer, J. R.; Gay, Y. J.; Desimone, J. M.; Khan, S. A. J Polym Sci Part B: Polym Phys 2000, 38, 3168.
14. Xue, A.; Tzoganakis, C. SPE ANTEC 2003, 61, 2276.
15. Wingert, M. J.; Shukla, S.; Koelling, K. W.; Tomasko, D. L.; Lee, L. J. Ind Eng Chem Res 2009, 48, 5460.
16. Williams, M. L.; Landel, R. F.; Ferry, J. D. J Am Chem Soc 1955, 77, 3701.
17. Penwell, R. C.; Porter, R. S. J Polym Sci Part A-2: Polym Phys 1971, 9, 463.
18. Chow, T. S. Macromolecules 1980, 13, 362.
19. Flichy, N. M. B.; Lawrence, C. J.; Kazarian, S. G. Ind Eng Chem Res 2003, 42, 6310.
20. Oh, J.-H.; Lindt, J. T. SPE ANTEC 2005, 63, 2555.
21. Oh, J.-H.; Lindt, J. T.; Ottoy, M. H. SPE ANTEC 2002, 60, 1920.
22. Zeng, C.; Han, X.; Lee, L. J.; Koelling, K. W.; Tomasko, D. L. Adv Mater 2003, 15, 1743.
23. Han, X.; Zeng, C.; Lee, L. J.; Koelling, K. W.; Tomasko, D. L. Polym Eng Sci 2003, 43, 1261.
24. Shen, J.; Zeng, C.; Lee, L. J. Polymer 2005, 46, 5218.
25. Shen, J.; Han, X.; Lee, L. J. J Cell Plast 2006, 42, 105.
26. Guo, Z.; Yang, J.; Wingert, M. J.; Tomasko, D. L.; Lee, L. J.; Daniel, T. J Cell Plast 2008, 44, 453.
27. Wang, Y.; Xu, J.; Bechtel, S. E.; Koelling, K. W. Rheol Acta 2006, 45, 919.
28. Dreisbach, F.; Seif, R.; Loesch, H. W. J Therm Anal Calorim 2003, 71, 73.
29. Sanchez, I. C.; Lacombe, R. H. Macromolecules 1978, 11, 1145.
30. Sato, Y.; Takikawa, T.; Takishima, S.; Masuoka, H. J Supercrit Fluids 2001, 19, 187.
31. Herbst, A.; Harting, P. Adsorption 2002, 8, 111.
32. S. Gronauer. Ph. D. Dissertation, The Ohio State University: Columbus, OH, 2007.
33. Cox, W. P.; Merz, E. H. J Polym Sci 1958, 28, 619.
34. Doraiswamy, D.; Mujumdar, A. N.; Tsao, I.; Beris, A. N.; Danforth, S. C.; Metzner, A. B. J Rheol 1991, 35, 647.
35. Kinloch, I. A.; Roberts, S. A.; Windle, A. H. Polymer 2002, 43, 7483.
36. Kohli, A.; Chung, N.; Weiss, R. A. Polym Eng Sci 1989, 29, 573.
37. Lam, Y. C.; Jiang, L.; Yue, C. Y.; Tam, K. C.; Hu, X. J Polym Sci Part B: Polym Phys 2003, 42, 302.
38. Siegmann, A.; Dagan, A.; Kenig, S. Polymer 1985, 26, 1325.
39. Zhao, R.; Macosko, C. W. J Rheol 2002, 46, 145.